New Scans and Data Visualisation on ROTAX

W. Schmidt[1,2], H. Tietze-Jaensch[1,2,3], R. Geick[1]

1.) Physikalisches Institut der Universität Würzburg, Am Hubland, 8700 Würzburg, F.R.G.
2.) ISIS Science Division, Rutherford Appleton Lab., Chilton OX11 0QX, U.K.
3.) Institut f. Festkörperforschung, KFA Jülich, Pf. 1913, 5170 Jülich, F.R.G.

For the rotating analyser crystal spectrometer ROTAX we have developed a new class of scans through $(\vec{Q},\omega)$-space which will considerably enhance the flexibility of the instrument. We will show the principles of these scans and discuss their advantages and limitations.
Further we will present new developments in visualisation and interpretation of detector data based on the 2-dimensional (time versus position) display of the JULIOS scintillation detector.

1.) Introduction

The spectrometer ROTAX uses a non-uniformly spinning crystal analyser for the neutrons scattered by a single crystal sample. The programmable motion of this analyser enables the user to scan different paths through $(\vec{Q},\omega)$-space of the sample. In this paper we will concentrate on new developments in scan construction for the analyser and the visualisation of the corresponding data on the detector. A general description of the instrument, its performance and current status can be found in [1].
The various possibilities to construct different time-of-flight scans are the key to the flexibility of ROTAX. So far several types of scans have been introduced where a particular value, e.g. the energy transfer, is kept constant. Concerning paths along a given Q-direction we have presented the 'const.-ψ' scan ($\psi = \sphericalangle(\vec{k}_i,\vec{Q})$) to measure e.g. longitudinal phonons [2-4].
However, there is no restriction to use only those scan types. Instead, Q-scans can be performed in a much more generalized form that are feasible within the limits of the analyser drive:
In principle, the spectrometer can perform a scan along any Q-direction with respect to a chosen Q-vector. This makes it possible to scan linearly through a particular point in $(\vec{Q},\omega)$-space along a selected direction, like a symmetry axis of the crystal. As a special case we should mention the 'transverse-q' scan where the scan direction is perpendicular to a chosen Q-vector, e.g. to measure transversal phonons.
For these "linear Q-scans" we will discuss the accessible $\vec{Q}$- and $\hbar\omega$-range in accordance with geometrical factors and the limitations in the dynamics of the analyser drive.
In addition to new scan constructions we will present new developments to visualize detector data in combination with real motor performance data.

The JULIOS scintillation detector on ROTAX gives a 2-dimensional data display, time-of-flight versus position. Due to the unambiguous scattering conditions on ROTAX, these detector coordinates can be expressed in terms of $\vec{Q}$ and $\hbar\omega$, and thus, projections of the reciprocal lattice of the sample or contour lines of the energy transfer can be plotted in the same display. Furthermore, the time-of-flight scan trajectory is also transferred to these coordinates.
This simultaneous observation of detector data within the projection of $(\vec{Q},\omega)$-space and the analyser scan onto the same display provides a valuable and effective help in preparing meaningful scans on ROTAX and judging the gathered data afterwards.

2.) Principles of the linear Q-scans

a) Definitions and basic relations

Before the possibilities of these Q-scans are discussed within motor dynamics and physical relevance we introduce the variables and definitions that are needed for further considerations.
The reciprocal lattice ($\vec{Q}$-space) of the sample is usually described in terms of Miller indices (h,k,l). Concerning the scattering plane these vectors can be transformed to a cartesian coordinate system with axes Q_x and Q_y. The Q_x-direction (a symmetry direction of the sample) is used as a reference with respect of the incoming neutrons ($\vec{k}_i$) defining the angle $\Omega = \measuredangle(\vec{Q}_x,\vec{k}_i)$ as the orientation angle of the reciprocal lattice in the spectrometer set-up. Further we refer to the angles $\psi = \measuredangle(\vec{Q},\vec{k}_i)$ and $\varphi = \measuredangle(\vec{k}_f,\vec{k}_i)$, the scattering angle at the sample. Fig. 1 shows the details. It should be noted that all angles are counted positive when pointing anti-clockwise.

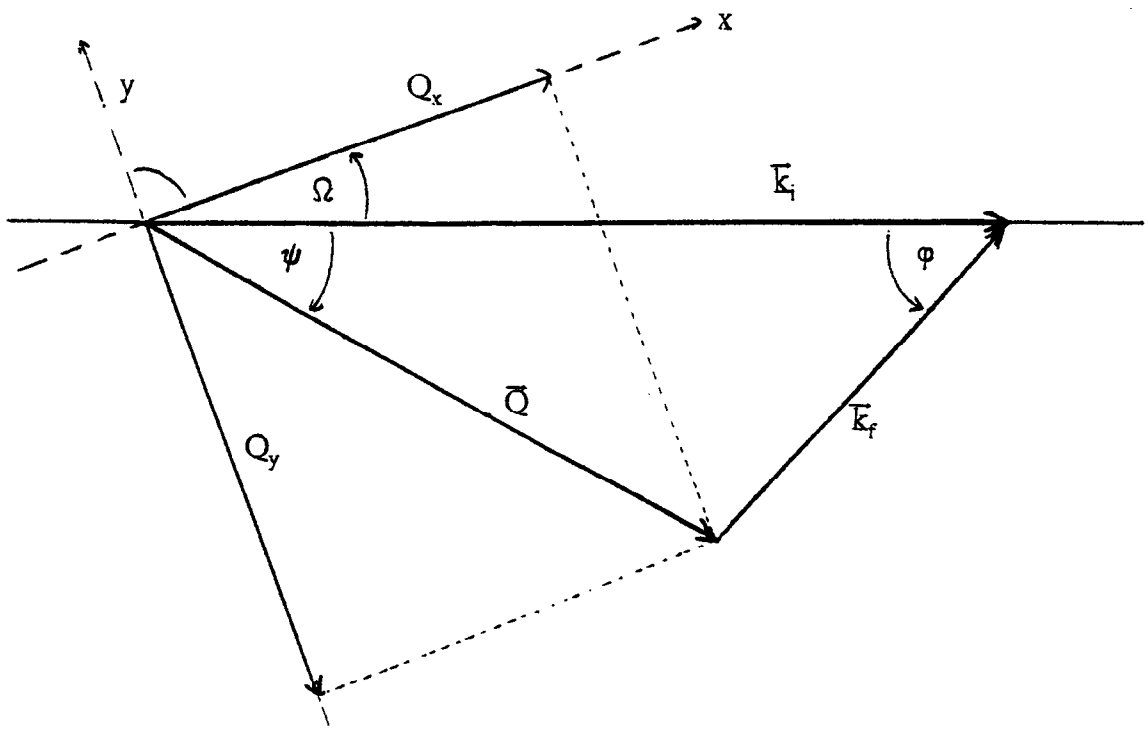

Fig. 1: Definition of the coordinate system in reciprocal space with the relevant angles.

From fig. 1 we deduce the basic relationship between Q, k_i and k_f :

$$\begin{aligned} Q_x &= Q \cdot \cos (\psi - \Omega) = k_i \cdot \cos \Omega - k_f \cdot \cos (\varphi - \Omega) \\ Q_y &= Q \cdot \sin (\psi - \Omega) = - k_i \cdot \sin \Omega - k_f \cdot \sin (\varphi - \Omega) \end{aligned} \tag{1}$$

For further use we will also need the following definitions for time-of-flight and Bragg angle of the analyser:

$$t_i = m_n L_i / \hbar k_i \qquad (L_i = \text{distance moderator to sample}) \tag{2}$$

$$t_a = m_n L_a / \hbar k_f \qquad (L_a = \text{distance sample to analyser}) \tag{3}$$

$$\sin \Theta_A = \pi / d_A k_f \qquad (d_A = \text{d-spacing of the analyser}) \tag{4}$$

Now, a linear Q-scan is defined by two vectors: A starting point ($\vec{Q}_0$) and the direction to be scanned ($\vec{Q}_{sc}$). Both may be given in (h,k,l)-values or directly in the x-y-coordinate system given above. In these coordinates the two vectors define the angles α and β as shown in fig. 2 .

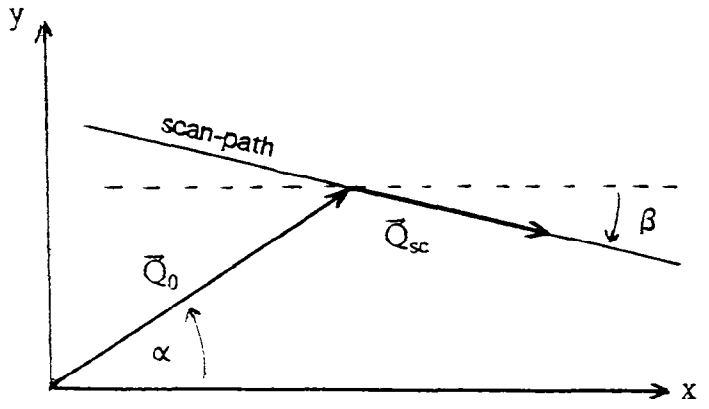

Fig. 2: Definition of the angles α and β for start point $\vec{Q}_0$ and scan direction $\vec{Q}_{sc}$.

In order to perform the scan we have to vary just one value, the size of $\vec{Q}_{sc}$. This fact is expressed by a scan parameter p in the following way:

$$Q_{sc}(p) = p \cdot Q_0 \tag{5}$$

With the angles from fig. 2 we then get a general expression for $\vec{Q}$ along the scan in dependence of p:

$$\begin{aligned} Q_x(p) &= Q_0 \cdot (\cos \alpha + p \cdot \cos \beta) \\ Q_y(p) &= Q_0 \cdot (\sin \alpha + p \cdot \sin \beta) \end{aligned} \tag{6}$$

The starting point $\vec{Q}_0$ is included in these equation for p = 0. A scan can be performed from a value $p_{min} < 0$ to $p_{max} > 0$ which will be given by the geometrical spectrometer set-up and limitations in the dynamics of the analyser drive.

Combining eq. 6 with eq. 1 yields the variation of k_i and k_f during the scan :

$$\begin{aligned} k_i(p) &= - Q_0 \cdot [\sin (\alpha + \Omega - \varphi) + p \cdot \sin (\beta + \Omega - \varphi)] / \sin \varphi \\ k_f(p) &= - Q_0 \cdot [\sin (\alpha + \Omega) + p \cdot \sin (\beta + \Omega)] / \sin \varphi \end{aligned} \tag{7}$$

For a given set of angles (α, β, Ω, φ) these equations can be used to determine the principle range for p and thus the scan length. A chosen time window for t_i yields the possible k_i-range (eq. 2) while the k_f-range is given by the possible analyser angles Θ_A (eq. 4). Using these limitations for k_i and k_f in eq. 7 we easily get the limits for p as well.
Further, from eq. 7 we can derive an expression for the energy transfer $\hbar\omega$ during a scan:

$$\hbar\omega(p) = -\hbar^2/2m_n \cdot Q_0^2 \cdot [\sin(2\alpha + 2\Omega - \varphi) + 2p \cdot \sin(\alpha + \beta + 2\Omega - \varphi) + p^2 \cdot \sin(2\beta + 2\Omega - \varphi)] / \sin\varphi \quad (8)$$

This equation may also be used to determine a range for p by setting lower and upper limits for $\hbar\omega$ to establish reasonable energy transfer values during a chosen scan.
Besides the range of p these equations for k_i, k_f and $\hbar\omega$ provide a guideline for the choice of the geometrical set-up: The user may wish specific values for the wave-vectors or the energy transfer at the starting point $\vec{Q}_0$. Thus, setting p=0, eq. 7 and 8 yield conditions between the angles α, Ω and φ. If, for example, we want $\hbar\omega = 0$ at $\vec{Q}_0$ we get the condition $2\alpha + 2\Omega - \varphi = n \cdot \pi$ from eq. 8.
In addition, even the variation of the energy transfer with respect to the scan direction can be used as a selection rule for the angles:

$$d(\hbar\omega)/dQ_{sc} = (d(\hbar\omega)/dp) / (dQ_{sc}/dp) = (d(\hbar\omega)/dp) / Q_0 \quad (9)$$

b) Motor dynamics

So far we have derived the basic equations and principle limitations for linear Q-scans. Another important consideration is the dynamics of the analyser drive, or in other words, can the motor drive perform the necessary rotation within its technical limits ?
In order to answer this question we have to look at motor speed and angular acceleration, i.e., the derivatives of Θ_A with respect to time. At this place we will not go through all the mathematics but instead give a short outline of the procedure and present the result for the motor speed as an example. This result is a good startpoint for discussion as well.

The arrival time t_A of the neutrons at the analyser is given by the sum $t_i + t_a$ (eq. 2,3) and, like the analyser angle, it is expressed in dependence of the scan parameter p :

$$\Theta_A = \Theta_A(k_f(p)) \quad \text{and} \quad t_A = t_i(k_i(p)) + t_a(k_f(p)) \quad (10)$$

So we can evaluate the derivatives

$$d\Theta_A/dp = d\Theta_A/dk_f \cdot dk_f/dp \quad \text{and}$$
$$dt_A/dp = dt_i/dk_i \cdot dk_i/dp + dt_a/dk_f \cdot dk_f/dp \quad (11)$$

as well as

$$d\Theta_A/dp = d\Theta_A/dt_A \cdot dt_A/dp \quad \text{with} \quad d\Theta_A/dt_A = \omega_A \quad . \quad (12)$$

A combination of these equations yields an expression for the motor speed ω_A.

Similarly further derivatives can be calculated, too. For ω_A we get:

$$\omega_A = (\pi \hbar / m_n L_i d_A) \cdot [\cos \Theta_A \cdot (\zeta + \gamma^2 \cdot x)]^{-1} \qquad (13)$$

with

$$x = \sin (\beta + \Omega - \varphi) / \sin (\beta + \Omega) \ , \ \zeta = L_a/L_i \ , \ \gamma = k_f/k_i \qquad (14)$$

Apart of the dependencies of Θ_A, k_f and k_i this equation shows a dramatic influence of the parameter x which absolute value can range from zero to infinity. We will discuss the two resulting extrema for ω_A :
First, eq. 13 shows that the term in square brackets vanishes for $x = - \zeta/\gamma^2$, i.e., we get very high speeds around that x-value which is approximately around zero since ζ is very small ($\zeta \approx 0.03$). Thus no scans are possible in a range around $\beta \approx \varphi - \Omega$.
In terms of physics: All scattered neutrons during the scan would arrive at the analyser at one specific time.
On the other hand, we may choose $\beta = - \Omega$ which yields infinity for x and correspondingly $\omega_A = 0$. Thus the analyser stands still and all scattered neutrons during the scan must have the same energy. This is confirmed by eq. 7 where $\beta = \varphi - \Omega$ yields k_f independent of p. In fact, this mode is used on PRISMA [5].
These considerations also hold for the higher order derivatives of Θ_A since they contain the square bracket term from eq. 13 as well. But nevertheless, the motor limits for these values must be checked for each scan, especially the angular acceleration is the limiting factor rather than the speed since this parameter is directly related to the necessary motor current. In total, all the limiting factors are checked automaticly in the scan construction program so that the user always gets the maximum length of a chosen scan within the technical limits.

c) Examples

The following figures will show some examples of possible scans using an aluminium sample (lattice constant = 6.22 Å) and a germanium analyser (4,0,0-reflection, d_A = 1.414 Å). The lengths (L_i = 14.1 m, L_a = 0.66 m) are realised on ROTAX.
The fig. 3a and 3b both show the reciprocal lattice of the sample in relative units (h,0,0 and 0,k,0) where we take the first vector as reference direction ($\alpha = 0$). Also shown are constant energy lines to get an estimate which energy range the scans cover. The scan paths themselves are drawn for different angles β as solid lines which spread out from Q_0. The step width for β is 1° in fig. 3.
In addition to the technical limitations we have restricted the scan length to an energy transfer interval of -20 meV $< \hbar\omega <$ 200 meV. Therefore the scan paths either end at the corresponding energy lines or - if shorter - the motor dynamics determines their lengths. The accessible k_i- and k_f-range is also included which can partly be seen as dashed lines.
According to the discussion of the influence of β on the motor speed we have indicated the directions $\beta = - \Omega$ (PRISMA mode) and $\beta = \varphi - \Omega$ (infinite speed). Both figures show clearly the gap around $\beta = \varphi - \Omega$ while for $\beta = - \Omega$ only the chosen energy interval determines the scan length.

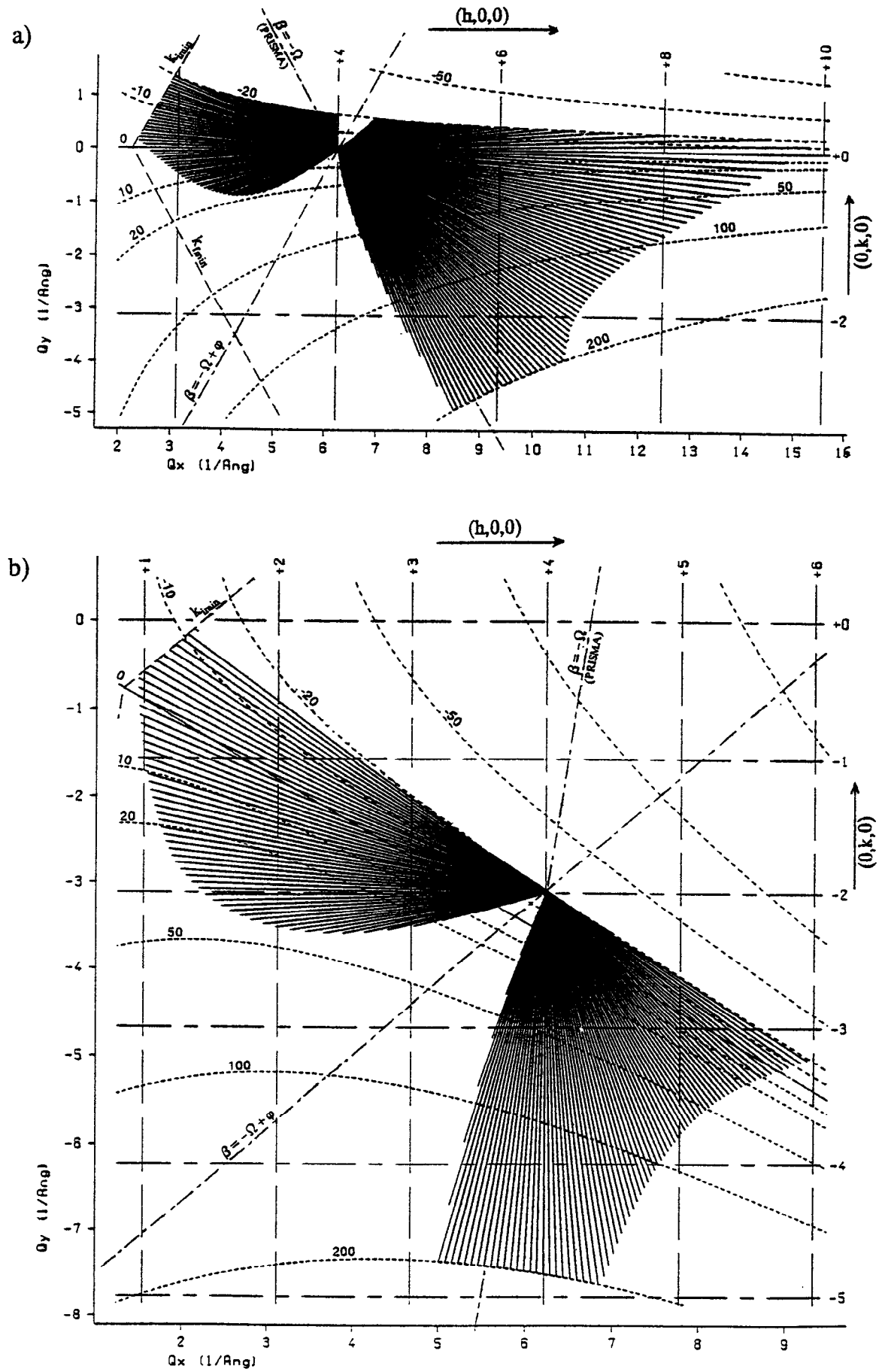

Fig. 3a,b: Feasible scan paths (solid lines) in reciprocal space for two different configurations. The dotted lines show the energy transfer in meV.

3a) $\alpha = 0°$, $\varphi = -60°$, $\Omega = 60°$, 3b) $\alpha = -25.6°$, $\varphi = -40°$, $\Omega = 100°$

Fig. 3a shows a configuration with $\vec{Q}_0$ = (4,0,0), thus α = 0°, and φ = - 60°, Ω = 60° which is favourable for scans with a low energy transfer pointing approximately along the (1,0,0)-direction. In fact we have chosen $\hbar\omega(p=0) = 0$ which results from $2(\alpha+\Omega)-\varphi$ = 180° here (cf. eq. 8) and thus we are able to include an elastic scan path as well. Concerning higher energy transfers one may choose a scan along (1,-1,0).
Instead fig. 3b shows a quite different behavior. Here we have set $\vec{Q}_0$ = (4,-2,0), thus α = - 25.6°, and φ = - 40°, Ω = 100°. Scans may be chosen around (1,-1,0)-direction with low energy transfer while scans with higher $\hbar\omega$-values are both possible along (1,0,0) and (0,1,0).
These two examples shall demonstrate that we get a wide range of different scan directions and different energy ranges. Certainly the technical limits of the analyser drive cut out some regions but with a proper set-up there will always be a possibility for a desired $\vec{Q}$ and energy range.

2.) Data visualisation

a) The JULIOS display

The ROTAX instrument uses the JULIOS scintillation detector from KfA Jülich [6]. This detector provides a 2-dimensional display: Position channels in the horizontal direction, time-of-flight channels in the vertical.
In relation to the analyser, each position channel corresponds to a specific Bragg angle there and can therefore be related to a well-defined k_f. Thus, when k_f is known, each time channel can be used to calculate also k_i. Fig. 4 shows the basic geometry with all parameters. The orientation of the detector is defined by a reference channel n_{x0} with a corresponding angle $2\Theta_{A0}$.

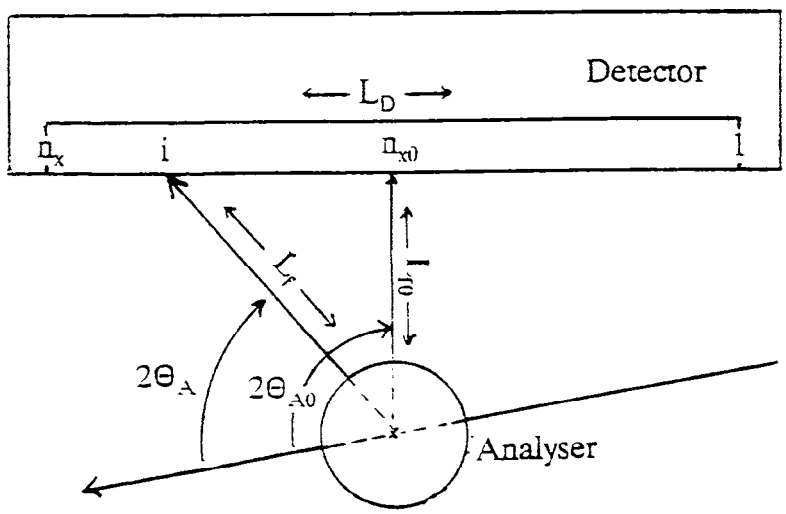

Fig. 4: Definitions of lengths and angles between analyser and detector position channels.

For a specific position channel i we get from the geometry

$$L_{f0} \cdot \tan (2\Theta_A(i) - 2\Theta_{A0}) = L_D \cdot (i - n_{x0})/n_x \quad (15)$$

$$L_f(i) = L_{f0} / \cos (2\Theta_A(i) - 2\Theta_{A0}) \quad (16)$$

$$k_f(i) = \pi / | d_A \cdot \sin \Theta_A(i) | \quad (17)$$

The time channels (from 1 to n_y) correspond to a user-chosen time window reaching from t_1 to t_2. For a specific time channel j we then get the total time-of-flight

$$t(j) = t_1 + (t_2 - t_1) \cdot j / n_y \quad (18)$$

and with eq. 17 the incident time-of-flight and k_i :

$$t_i(i,j) = t(j) - m_n \cdot (L_f(i) + L_a) / \hbar k_f(i) \quad (19)$$

$$k_i(i,j) = m_n L_i / \hbar t_i(i,j) \quad (20)$$

b) Projections of $(\vec{Q},\omega)$-space

As we have seen in the previous section we can relate every pixel (i,j) of the detector display to a pair $k_i(i,j)$ and $k_f(i)$. Therefore we are able to calculate the Q-components (eq. 1) and the energy transfer for each pixel as well. This is used to create a grid of two chosen $\vec{Q}$-vectors and energy lines similar to fig. 3. However, due to the non-linearities in eq. 15 to 20 a rectangular reciprocal lattice (as the aluminum grid in fig 3) appears highly deformed. Thus, different Brillouin-zones of actually the same size cover more or less pixels on the detector screen depending on their related values in position and time. In addition, as done in fig. 3, any scan can be plotted in the same display.
This provides a helpful tool for the user:
- The user knows in advance how the reciprocal lattice, energy transfer and the scan are related with the grid of detector channels. The size of a specific Brillouin-zone or the density of constant-energy lines gives an estimate for the expected resolution.
- During an experiment the user can easily interprete intensities, not only along the scan path but also near or perpendicular to it. This shows immediately how far a measured excitation is extended into the Brillouin-zone or how broad it is in energy.

c) Application

All these theoretical considerations have been applied to inelastic data obtained with ROTAX [1,4] using an aluminum sample. In a scan along (1,0,0)-direction we have measured longitudinal phonons simultaneously in two different Brillouin-zones. Fig. 5 shows the results with the projection of the reciprocal lattice, energy transfer and the scan path into the display. Instead of the real colour display three different count-rate levels are selected. The graphics shows the defacing of the quadratic lattice. The zone around (2,0,0) is much larger on the display than the next zone around (4,0,0). But the display shows also interesting details confering the information perpendicular to the scan. The inelastic scattering intensity distributions are slightly asymmetric off the scan path and, with greater distance from the zone centers, tilted towards higher values of $\hbar\omega$. This is, in fact, a resolution effect, arising form the dispersion of the phonon branches, and made visible as a whole directly on the detector screen.

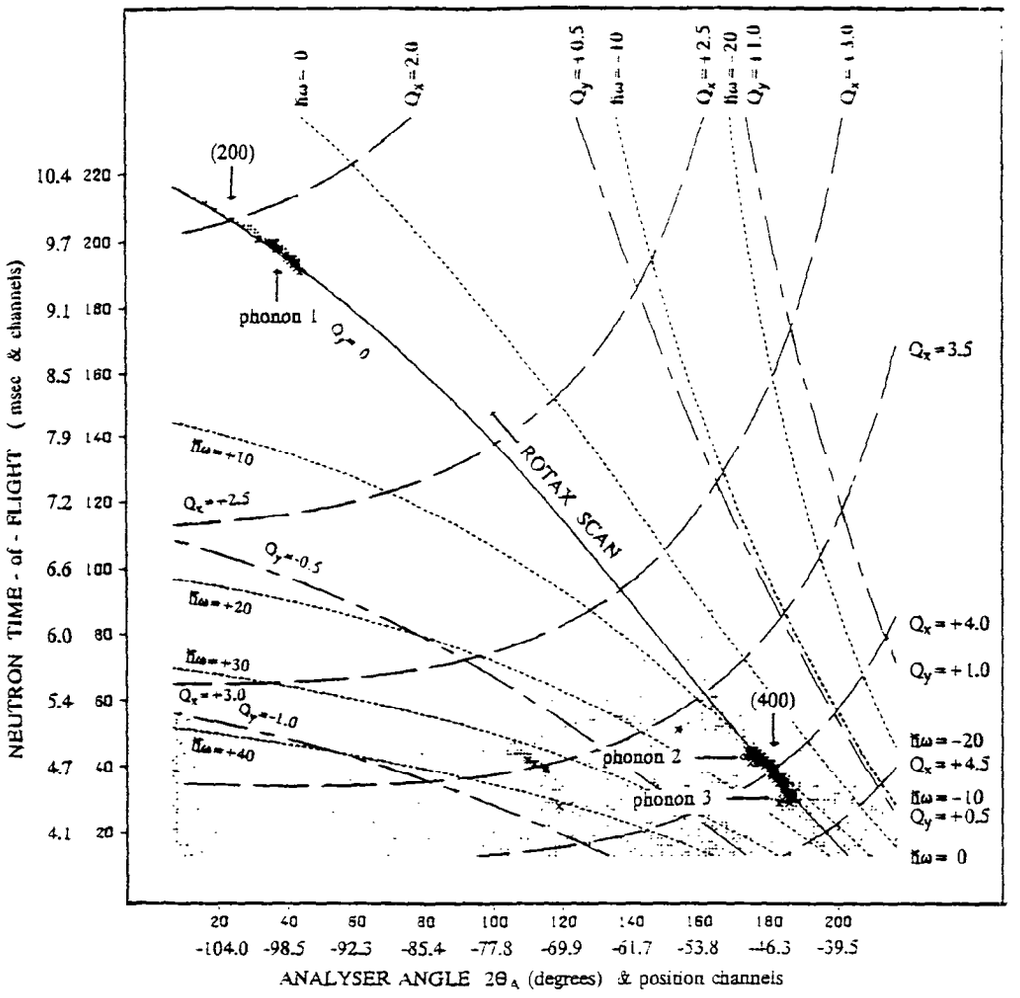

Fig. 5: The detector display with inelastic data and the projection of $(\vec{Q},\omega)$-space. The energy transfer is given in meV, the reciprocal lattice in relative units (as in fig. 3).

Acknowledgement

ROTAX is funded by the BMFT under contract number 03-GE3-WUE.

References

[1] H.Tietze-Jaensch, W. Schmidt, R. Geick
Proc. ICANS XII, Session A2 (1993)

[2] R. Geick, H. Tietze; Nucl. Instr. Methods A **249** (1986) 325

[3] H. Tietze, R. Geick
Proc. Int. Collab. Advanced Neutron Sources ICANS IX 1986, CH-Villigen, Switzerland, SIN-rep. 40926, 389 (1987)

[4] H. Tietze, W. Schmidt, R. Geick, U. Steigenberger, H. Samulowitz;
Proc. Int. Collaboration on Advanced Neutron Sources ICANS XI 1990, KEK Japan, KEK report 90-25, 774 (1991)

[5] U. Steigenberger, M. Hagen, R. Caciuffo, C. Petrillo, F. Cilloco and F. Sacchetti
1990 RAL-90-004 and Nucl. Inst. and Meth. **B53** (1991) 87

[6] E. Jansen, W. Schäfer, A. Szepesvary, R. Reinartz, H. Tietze, G. Will, K.D. Müller, U. Steigenberger;
Proc. Int. Conf. on Neutron Scattering ICNS 91, Oxford (1991),
Physica B **180 & 181** (1992) 917